DOI: 10.14256/JCE.1311.2015

Građevinar 9/2015

Primljen / Received: 31.3.2015.
Ispravljen / Corrected: 9.7.2015.
Prihvaćen / Accepted: 12.9.2015.
Dostupno online / Available online: 10.10.2015.

Cable oscillations due indirect excitation

Authors:

Marija Demšić, MCE
University of Zagreb
Faculty of Civil Engineering
mnikolic@grad.hr

Assist.Prof. Verica Raduka, PhD. CE
University of Zagreb
Faculty of Civil Engineering
verar@grad.hr

Original scientific paper

Marija Demšić, Verica Raduka

Cable oscillations due indirect excitation

An analytical cable oscillation model is formulated for inhomogeneous boundary conditions taking into account quadratic and cubic nonlinearities of the system. The reduced system is solved by numerical integration and, for the case of external and parametric oscillations, by the multiple scales perturbation method. The comparison of solutions with numerical model results is based on the finite difference model and the predictor-corrector algorithm for time integration of equation systems.

Key words:
cables, nonlinear oscillations, method of multiple scales

Izvorni znanstveni rad

Marija Demšić, Verica Raduka

Oscilacije kabela uslijed indirektne pobude

U radu je formuliran analitički model oscilacija kabela za nehomogene rubne uvjete pri čemu su uzete u obzir kvadratne i kubne nelinearnosti sustava. Oblikovan je reducirani sustav koji je riješen numeričkom integracijom, te za slučaj prisilnih i parametarskih oscilacija perturbacijskom metodom višestrukih skala. Dobivena rješenja uspoređena su s rješenjima numeričkog modela pri čemu je korištena metoda konačnih diferencija i algoritam prediktor-korektor za vremensku integraciju sustava jednadžbi.

Ključne riječi:
kabeli, nelinearne oscilacije, metoda višestrukih skala

Wissenschaftlicher Originalbeitrag

Marija Demšić, Verica Raduka

Durch indirekte Anregung bewirkte Kabelschwingungen

In dieser Arbeit wird ein analytisches Model zur Beschreibung von Kabelschwingungen bei nicht homogenen Randbedingungen unter Berücksichtigung quadratischer und kubischer Nichtlinearitäten aufgestellt. Ein reduziertes System wurde aufgestellt und durch numerische Integration gelöst, sowie für den Fall erzwungener und parametrischer Schwingungen mittels der Multi-Skalen-Methode betrachtet. Die Ergebnisse sind den auf einem numerischen Modell beruhenden Resultaten gegenübergestellt, wobei die Finite-Differenzen-Methode und der Prädiktor-Korrektor-Algorithmus zur Zeitintegration des Gleichungssystems angewandt wurden.

Schlüsselwörter:
Kabel, nichtlineare Schwingungen, Methode mehrfacher Skalen

1. Introduction

Thanks to an efficient load transfer, long span cables are often used as main load-carrying parts in modern structures (cable stayed bridges, cable nets, masts, marine platform cables, etc.). In addition to their extensive use in civil engineering, they are also utilised in the traffic, mechanical, and electrical engineering applications (transmission lines, cableways, mooring lines, etc.). The load is transmitted in cables by tensile forces and involves a change in geometry and, therefore, cables have a highly nonlinear response. While response due to static actions can be determined quite well using physical models and numerical analyses, the effects of dynamic action are more difficult to predict. Long span cables are prone to large amplitude oscillations due to their great flexibility, small mass, and low damping characteristics. This can result in the loss of usability or in serious damage to cables or their anchors [1]. Basic dynamic characteristics of cables depend on the initial static profile, tension, and cable span. Depending on static profile, a distinction can be made between the small-sag and large-sag cables, i.e. between parabolic cables and catenaries. Analytic solutions for natural frequencies and mode shapes are available for small-sag cables because, in this case, the continuous formulation is greatly simplified by parabolic approximation, while discrete formulations and numerical methods are used for large-sag cables [2].

The fundamental dynamics of parabolic cables, which takes into account cable stretching and inelastic changes in geometry, was clarified by Irvine and Caughey in 1974 [3, 4]. They defined frequency spectra and the frequency crossover phenomenon by unifying elastic and geometric effects via the so called cable parameter $\lambda^2 = L(mgL\cos\varphi/H\sec\varphi)^2/(H\sec\varphi L_e/EA)$, also known as the Irvine parameter. By introducing the geometric parameter $\nu = d/L = mgL/(8H\sec^2\varphi)$ (sag to span ratio) and the cable elasticity parameter $\eta = AE/(H\sec\varphi)$, the cable parameter can be expressed as $\lambda^2 = 64\nu^2\eta \cdot L/L_e$. For cables with a very small self-weight to pretension force ratio, the quantity $L_e = L(1+8\nu^2)$, is only slightly greater than the cable span. Generally, the Irvine parameter λ^2 is more influenced by cable geometry than by stretching. To prevent violation of parabolic assumption of a static profile, the sag to span ratio has to be 1/8 or less. Therefore, higher cable parameter values are related to materials with a high modulus of elasticity. Most cables used in technical applications have very small values of parameter λ^2. Parameter λ^2 strongly influences symmetric mode frequencies of parabolic cables. The dimensionless frequency value $\bar{\omega}$ is defined by the following transcendental equation [4]:

$$\frac{\bar{\omega}}{2} - \tan\left(\frac{\bar{\omega}}{2}\right) = \frac{4}{\lambda^2}\left(\frac{\bar{\omega}}{2}\right)^3 \quad (1)$$

For values $\lambda^2 < 4\pi^2$, the first symmetric mode shape has no internal nodes, while two internal modes appear for $\lambda^2 > 4\pi^2$, and the associated frequency is greater than the frequency of the first asymmetric mode. Changes in symmetric modes frequency values can be seen in Figure 1a, which shows a frequencies spectrum. It can be noted that the frequency crossover also occurs in higher symmetric modes. The asymmetric mode frequency values do not depend on the parameter λ^2 and their dimensionless value is:

$$\bar{\omega} = 2n\pi, \ n = 1, 2, 3 \ldots \quad (2)$$

Subsequent research conducted with analytic models of inclined cables showed that veering phenomena occur near crossover points, as shown in Figure 1b [5, 6]. Inclined cables with a small self-weight to tension ratio are more influenced by the static profile dissymmetry, which is particularly noticeable in the region where the system frequency values are almost equal. Hybrid mode shapes are formed in this region, as confirmed by experimental and numerical studies [7]. After a further increase of the parameter λ^2, the frequencies are once again separated, and so the crossover never occurs. Outside of the veering region, the modes are not "fully" symmetric and asymmetric, although they are very similar to them.

Partial differential equations of cable motion include quadratic and cubic nonlinearities resulting from initial cable curvature and stretching. Solutions to such equations can be determined by approximate numerical or approximate analytic methods.

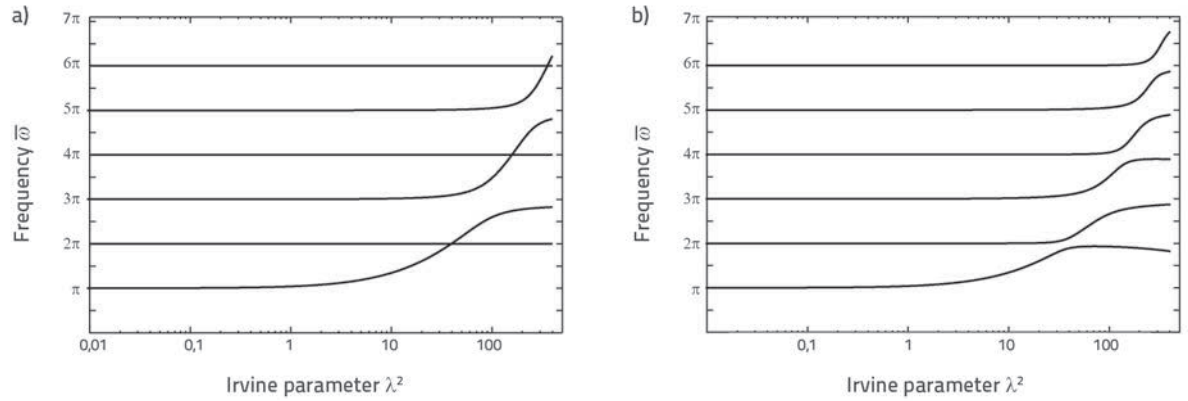

Figure 1. Cable frequencies spectrum: a) horizontal / highly pretension cables; b) inclined cables

In the analytic analysis, solutions are often postulated by the discretisation $w(x,t) = \Sigma q_n(t)\ \phi_n(x)$, where the displacement field is assumed *a priori* using trial functions $\phi_n(x)$ after which the method of weighted residual is applied. In this way, the basic differential equation and boundary conditions are reduced to the system of ordinary differential equations governing time independent functions $q_n(t)$. The Galerkin procedure is frequently used as a means of implementing the weighted residuals method in the analysis of cable dynamics. Linear cable modes are commonly used for trial functions because they satisfy the fundamental requirement that trial functions need to be members of a complete set of functions. Such mathematical formulation of cable motion corresponds to the Helmholtz-Duffing oscillator in the theory of dynamical systems [2]. Functions $q_n(t)$ can be determined numerically or by applying perturbation methods. Perturbation methods like Poincare-Lindstedt, Krylov-Bogoliubov-Mitropolskii, and the Method of Multiple Scales (MMS), are used for obtaining asymptotic solutions for a particular domain of system parameters in an analytic form. An analytic solution can also be determined using the Harmonic Balance Method (HMB) in which the function $q_n(t)$ is postulated through superposition of harmonic functions with unknown coefficients. In addition to being dependent on geometric nonlinearity, dynamic responses depend on initial conditions in a certain region of parameters. In this region, called the hysteresis region, more system response solutions are possible. The so-called jumps may occur in the hysteresis region, which leads to sudden changes in dynamic response due to an increase or decrease in the oscillation amplitude [14].

Dynamic excitation can act directly on cable, or indirectly through inhomogeneous boundary conditions, when oscillations are caused by support displacements induced by motion of the structure. For example, live load, wind load, or earthquake action, when applied on a cable stayed bridge, can cause very small frequent cable displacements at the connection between cables and the deck or pylon. Although this type of dynamic cable loading is often called parametric excitation in technical and scientific literature, it is more appropriate to refer to it as the indirect excitation since periodic displacements of supports generate external and/or parametric excitation on the cable.

Cable oscillations caused by external excitation are very often treated as a linear phenomenon and, because of a very low cable damping, oscillation amplitudes determined in this way can have extremely large values. Finite element models and simplified analytic models where cables are approximated with the taut wire model (only cubic nonlinearities) show that the activation of nonlinearities occurs quite quickly at very small damping values, which significantly limits the size of the oscillation amplitude [8].

The phenomenon of parametric oscillations is increasingly being recognised in the engineering practice, and so recommendations for the long span cable design provide basic guidelines for determination of the parametric resonance parameters domain and amplitude values (e.g. cable stays in [1]). In general, the parametric oscillation occurs if one of the system parameters, such as stiffness, changes during the oscillation, so that the excitation appears in the governing differential equation as a coefficient of an unknown function [14]. Parametric oscillations of cables are caused by tension variations due to longitudinal support displacement [1]. Analytic expressions for parametric oscillation amplitude values due to longitudinal motion of the cable anchorage are determined in paper [9] where a reduced cable model is formed. This model neglects cable curvature in the initial state and uses the HBM to obtain analytic solutions that are verified using the finite element model. The influence of vertical support motion on the parametric and external resonance, presented in [10], is analysed on nonlinear models of a vertical and horizontal cable, and the inclined cable response values are determined numerically. In paper [11], the HBM is used to determine analytic expressions for the second mode external resonance regions due to transverse motion on the support, and for the region of parametric resonance generated by the longitudinal support motion. An initial profile curvature and quadratic nonlinearities are neglected in the mathematical model. Though the finite element numerical investigation shows that the longitudinal component of the cable support motion also causes an external resonance [10], this is not included in analytic formulations of the mentioned studies.

In this paper, the mathematical model of cable oscillations that include quadratic and cubic nonlinearities is reduced to a finite-degree-of-freedom model using the Galerkin method. The asymptotic solution of the one-degree-of-freedom system is obtained using the MMS technique. Analytic expressions for the resonance regions and amplitude values are derived. The local stability analysis of dynamic motion is conducted for the obtained solution. The equation of the reduced one-degree-of-freedom system is also solved by numerical integration in the Wolfram *Mathematica* software. A numerical model with the finite difference space discretization is formed to validate formulation of dynamic excitation by support motion, and to confirm the a priori assumed deformation shape as used in the analytic model. The time integration of the ordinary differential equations system is carried out by the Wolfram *Mathematica* in which the Predictor-Corrector algorithm is implemented.

2. Equations of motion

The cable is modelled as a one-dimensional linear-elastic continuum without the flexural, torsional, and shear rigidity. Assuming the use of a highly pretensioned cable, the parabolic assumption shows that $ds \approx dx$, and so the cable profile shown in Figure 2a for static equilibrium can be approximated with the function:

$$z(x) = \frac{m g L^2}{2H \sec^2 \varphi}\left(\frac{x}{L} - \frac{x^2}{L^2}\right) \tag{3}$$

where L is the cable span, m is the mass by unit length, φ is the cable inclination toward the horizontal axis, and H is the horizontal component of force [4].

The dynamic configuration of cables is determined by superposition of the rigid static profile and relative motion caused by cable deformation. The principle of virtual displacements is used for the determination of partial differential equations of cable motion shown in Figure 2b. Partial derivatives of functions with respect to the spatial and temporal coordinates are shown with common labels, that is $f' = \partial f(x,t)/\partial x$ and $\dot{f} = \partial f(x,t)/\partial t$. The effect of internal elastic forces on virtual displacements is equal to the cable strain energy, and its variation is only due to cable stretching:

$$\delta U = \int_0^L EA\,\bar{\varepsilon}\,\delta\bar{\varepsilon}\,dx \tag{4}$$

In the above expression, $EA\bar{\varepsilon}$ represents the elastic force of a differential segment obeying the Hooks law, while $\bar{\varepsilon}$ is the total deformation in the dynamic equilibrium position *p*:

$$\bar{\varepsilon} = \varepsilon_s + \frac{dp - ds}{ds} = \varepsilon_s + \left(\left(1+u'\right)^2 + \left(z'+w'\right)^2\right)^{1/2} - 1 \tag{5}$$

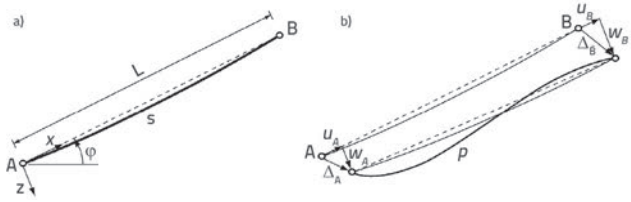

Figure 2. Cable model: a) static position; b) dynamic position

in which ε_s is the initial static strain, *u(x,t)* and *w(x,t)* are longitudinal and transverse components of relative displacement (Figure 3). It follows that variation of total strain is:

$$\delta\bar{\varepsilon} = \frac{\left(1+u'\right)\delta u' + \left(z'+w'\right)\delta w'}{\left(\left(1+u'\right)^2 + \left(z'+w'\right)^2\right)^{1/2}} \tag{6}$$

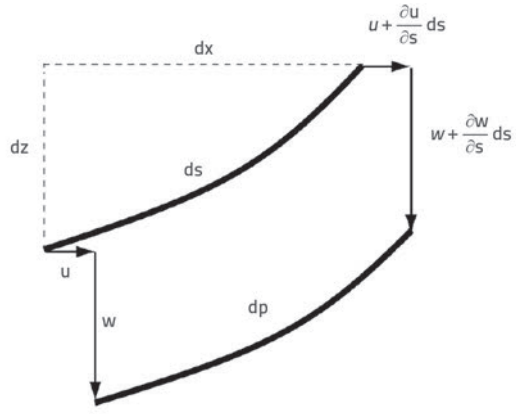

Figure 3. Differential cable segment in local coordinate system

Assuming that longitudinal displacements and static strain are small compare to transverse displacements, their higher order terms are neglected, and so the virtual work of internal forces is:

$$\begin{aligned}\delta U = &-\int_0^L \left[EA\varepsilon_s + EA\left(u' + zw' + \tfrac{1}{2}w'^2\right)\right]'\delta u\,dx \\ &-\int_0^L \left[EA\varepsilon_s z' + EA\varepsilon_s w' + EA\left(z'+w'\right)\left(u' + zw' + \tfrac{1}{2}w'^2\right)\right]'\delta w\,dx\end{aligned} \tag{7}$$

The virtual work done by the cable weight is:

$$\delta W_G = \int_0^L \left(-mg\sin\varphi\,\delta u + mg\cos\varphi\,\delta w\right)dx \tag{8}$$

The virtual work done by inertial forces is given by:

$$\delta W_i = -\int_0^L \left(m\ddot{u}_o\,\delta u + m\ddot{w}_o\,\delta w\right)dx - \int_0^L \left(m\ddot{u}\,\delta u + m\ddot{w}\,\delta w\right)dx \tag{9}$$

Functions $\ddot{u}_o(x,t)$ and $\ddot{w}_o(x,t)$ are components of the rigid body acceleration, while $\ddot{u}(x,t)$ and $\ddot{w}(x,t)$ are acceleration components due to deformation. Assuming vicious damping, the work done by these forces is:

$$\delta W_P = -\int_0^L \left(c\dot{u}\,\delta u + c\dot{w}\,\delta w\right)dx \tag{10}$$

According to the principle of virtual displacements, the overall work of all forces must vanish:

$$\delta\Pi = \delta U - \left(\delta W_G + \delta W_i + \delta W_P\right) \tag{11}$$

The expressions (7), (8), (9), (10) are substituted in (11) and the static equilibrium equations are taken into account. After separation of equations by displacement components, and using the relation $EA\varepsilon_s \approx H\sec\varphi$ for static force, the following Euler equations of motion are obtained:

$$\left[EA\left(u' + z'w' + \tfrac{1}{2}w'^2\right)\right]' = m\ddot{u}_o + m\ddot{u} + c\dot{u} \tag{12}$$

$$\left[H\sec\varphi\,w' + EA\left(z'+w'\right)\left(u' + z'w' + \tfrac{1}{2}w'^2\right)\right]' = m\ddot{w}_o + m\ddot{w} + c\dot{w} \tag{13}$$

Using the following substitutions, in which ξ is the coefficient of relative damping and $\bar{\omega}$ is the dimensionless natural frequency of linear mode:

$$\tilde{x} = \frac{x}{L},\ \tilde{w} = \frac{w}{L},\ \tilde{u} = \frac{u}{L},\ \tilde{z} = \frac{z}{L},\ \tilde{w}_o = \frac{w_o}{L},\ \tilde{u} = \frac{u_o}{L},$$
$$\bar{t} = \frac{t}{L}\sqrt{\frac{H\sec\varphi}{m}},\ \omega = \frac{\bar{\omega}}{L}\sqrt{\frac{H\sec\varphi}{m}},$$
$$\eta = \frac{AE}{H\sec\varphi},\ \mu = \xi\bar{\omega},\ \nu = \frac{mgL}{8H\sec^2\varphi},$$

the partial differential equations (12) and (13) and the equation (3) are transformed into the dimensionless form:

$$\left[\eta\left(\tilde{u}' + \tilde{z}'\tilde{w}' + \tfrac{1}{2}\tilde{w}'^2\right)\right]' = \ddot{\tilde{u}}_o + \ddot{\tilde{u}} + 2\mu\dot{\tilde{u}}, \tag{14}$$

$$\left[\tilde{w}' + \eta\left(\tilde{z}' + \tilde{w}'\right)\left(\tilde{u}' + \tilde{z}'\tilde{w}' + \tfrac{1}{2}\tilde{w}'^2\right)\right]' = \ddot{\tilde{w}}_o + \ddot{\tilde{w}} + 2\mu\dot{\tilde{w}} \tag{15}$$

$$\tilde{z}(\tilde{x}) = 4\nu\left(\tilde{x} - \tilde{x}^2\right) \tag{16}$$

In the following analysis, the tilde "~" and "–" signs are omitted for simplicity reasons.

In pretensioned steel cables, the speed of propagation of longitudinal waves is much greater than that of transverse waves. Consequently, the stretching of cable occurs nearly instantaneously or quasi-statically on the time scale of transverse motion [1, 2]. This is a commonly used assumption for the parabolic cable analysis in which inertia can be neglected in longitudinal direction, while the longitudinal component of motion in the equation (14) can be condensed. The assumption that cable stretching depends solely on current deformation is also in accordance with parabolic approximation. However, the assumption of quasi-static stretching is no longer valid if the response involves high-order elastic modes which exhibit substantial longitudinal displacements. Therefore, by taking into account the assumption of quasi-static cable stretching in equation (14), we neglect the inertia and damping:

$$\left[\eta\left(u' + z'w' + \tfrac{1}{2}w'^2\right)\right]' = 0 \tag{17}$$

Now, the equation (17) can directly be integrated as follows:

$$u' + z'w' + \tfrac{1}{2}w'^2 = e \tag{18}$$

Hence, the cable stretching $e=e(t)$ is only a function of the time variable. The equation of motion for the transverse direction is given by the expression:

$$\left[w' + \eta\left(z' + w'\right)e\right]' = \ddot{w}_o + \ddot{w} + 2\mu\dot{w} \tag{19}$$

2.1. Formulation of dynamic equation for indirect dynamic excitation

The function of support motion is harmonic with the frequency Ω and amplitudes Δ_A and Δ_B. Very small amplitudes, capable of causing large cable response amplitudes for certain frequencies, are assumed. All inertial effects in longitudinal direction are ignored due to the assumption that response will not involve elastic modes. Additional cable stretching generated by longitudinal displacement is taken into account. Boundary conditions in the longitudinal direction are:

$$\begin{aligned} u(0,t) &= u_A \cos\Omega t \\ u(1,t) &= u_B \cos\Omega t \end{aligned} \tag{20}$$

Taking into account these conditions, the expression (18) is integrated, and it follows that stretching can be determined from the equation:

$$e = \left(u_B - u_A\right)\cos\Omega t + \int_0^1 \left(z'w' + \tfrac{1}{2}w'^2\right)\mathrm{d}x \tag{21}$$

For very small sag to span ratio of pretension cables, the acceleration distribution $\ddot{w}_o(x,t)$ in transverse direction along the cable length can be approximated by the linear function:

$$\ddot{w}_o(x,t) = -(1-x)\Omega^2 w_A \cos\Omega t - x\Omega^2 w_B \cos\Omega t \tag{22}$$

To simplify expressions, it can be assumed that the support B is fixed, i.e. that $\Delta_B = 0$, and the support displacement amplitude A ($\Delta_A = \Delta$) is defined with longitudinal $u_A = \Delta_u$ and transverse $w_A = \Delta_p$ components. Once the support displacement conditions are introduced, the equation (19) for the transverse cable oscillation is given by:

$$\begin{aligned} &w'' + \eta\left(z'' + w''\right)\left(-\Delta_u \cos\Omega t + \int_0^1 \left(z'w' + \tfrac{1}{2}w'^2\right)\mathrm{d}x\right) = \\ &= \ddot{w} + 2\mu\dot{w} - (1-x)\Omega^2\Delta_p \cos\Omega t \end{aligned} \tag{23}$$

The equation (23) shows that the longitudinal support displacement generates parametric and external excitations, which cause transverse cable oscillations. The generation of external excitations is due to the curved shape of the system in static position so that, in the limit case of the taut wire model, the longitudinal support motion causes the parametric excitation only. Unlike the taut wire model, this model does not require initial disturbance to initiate parametric oscillation. The transverse component of support motion generates the external dynamic excitation only.

3. Analytic model

The Galerkin method for system reduction was used to form the analytic model. Low-order models with the one-degree-of-freedom can be used to highlight basic dynamic features of the nonlinear problem [2]. The function $w(x,t)$ is written as follows:

$$w(x,t) = \sum_n q_n(t)\,\phi_n(x) \tag{24}$$

In which $\phi_n(x)$ is the function of the n-th linear transverse mode shape [4], with the maximum amplitude normalization:

$$\phi_n(x) = \begin{cases} \dfrac{\cos\left(\frac{\omega_n}{2}\right)}{\cos\left(\frac{\omega_n}{2}\right)-1}\left(1-\tan\left(\frac{\omega_n}{2}\right)\sin\left(\omega_n x\right)-\cos\left(\omega_n x\right)\right), & n = 1,3,5\ldots \\ \sin\left(\omega_n x\right), & n = 2,4,6\ldots \end{cases} \tag{25}$$

Symmetric and asymmetric mode shapes are defined by the first and second functions, respectively. The corresponding frequencies are given by equations (1) and (2). After substituting expression (24) in equation (23), and after minimizing the residual, it follows that the equation of transverse oscillations is:

$$\begin{aligned} &\ddot{q}_n + 2\mu\dot{q}_n + \omega_n^2 q_n + \sum_{i,j}\Lambda_{n_{ij}} q_i q_j + \sum_{i,j,k}\Gamma_{n_{ijk}} q_i q_j q_k - k_n\Delta_u\, q_n \cos\Omega t = \\ &= p_n\Omega^2\Delta_p \cos\Omega t + \mathrm{h}_n\,\Delta_u \cos\Omega t \end{aligned} \tag{26}$$

The coefficients in equation (26) are determined by the following expressions:

$$\begin{aligned} m_n &= \int_0^1 \phi_n^2\,\mathrm{d}x, \\ \omega_n^2 &= \frac{1}{m_n}\left(\int_0^1 \phi_n'^2\,\mathrm{d}x + \eta\left(\int_0^1 z'\phi_n'\,\mathrm{d}x\right)^2\right), \\ \Lambda_{n_{ij}} &= \frac{\eta}{m_n}\left(\frac{1}{2}\int_0^1 \phi_i'\phi_j'\,\mathrm{d}x\int_0^1 z'\phi_n'\,\mathrm{d}x + \int_0^1 z'\phi_i'\,\mathrm{d}x\int_0^1 \phi_j'\phi_n'\,\mathrm{d}x\right), \\ \Gamma_{n_{ijk}} &= \frac{\eta}{2m_n}\int_0^1 \phi_i'\phi_j'\,\mathrm{d}x\int_0^1 \phi_k'\phi_n'\,\mathrm{d}x, \\ k_n &= \frac{\eta}{m_n}\int_0^1 \phi_n'^2\,\mathrm{d}x, \quad h_n = \frac{8\eta v}{m_n}\int_0^1 \phi_n\,\mathrm{d}x, \quad p_n = \frac{1}{m_n}\int_0^1 (1-x)\phi_n\,\mathrm{d}x. \end{aligned} \tag{27}$$

3.1. Asymptotic solution

By introducing labels for quadratic nonlinearities α_n and cubic nonlinearities δ_n, a general differential equation (26) for only one-degree-of-freedom can be written more compactly as follows:

$$\ddot{q}_n + 2\mu_n \dot{q}_n + \omega_n^2 q_n + \alpha_n q_n^2 + \delta_n q_n^3 - K_n q_n \cos\Omega t = P_n \cos\Omega t \quad (28)$$

Coefficients for external and parametric excitation amplitudes are:

$$\begin{aligned} P_n &= p_n \Omega^2 \Delta_p + \mathrm{h}_n \Delta_u \\ K_n &= k_n \Delta_u \end{aligned} \quad (29)$$

The MMS procedure is used to determine the asymptotic solution for equation (28). Perturbation methods are based on forming solutions via expansion of functions in which expansion members represent a correction of a basic non-perturbed solution. The expansion series is formed according to a small perturbation parameter ε. The first correction is small with respect to the basic solution; the second correction is small with respect to the first correction, and so on. The ordering is an unbreakable basic rule when we conduct perturbation calculations and form asymptotic solutions [12]. In this way, the system of equations suitable for successive solving is formed through perturbation hierarchy. To carry out the procedure, the equation of motion has to be written in a dimensionless form, after which a small parameter ε is selected to form an asymptotic solution. If the small parameter suitable for the ranking does not appear explicitly in the equation, then the physical system/problem has to be modelled. Understanding the physical nature of a nonlinear problem in the modelling procedure is of fundamental importance for its correct mathematical formulation. The ordering of terms in a differential equation can have a decisive influence on the structure of the final asymptotic solution, with clear connotations to the accuracy and physical relevance [13]. In this case, we can make use of an *artificial* parameter popularly called the *bookkeeping parameter* [14,15]. Such a parameter is used to introduce an implicit assumption about the influence of nonlinear coefficients, damping, and excitation, on the system's response [13]. If the substitution $q = \varepsilon\hat{q}$, is introduced in a differential equation (28), nonlinearities will generate the terms of the order $O(\varepsilon^3)$. In order to enable interference of the damping, excitation and nonlinear terms at the same level of perturbation hierarchy, the damping must be scaled to $\mu_n = \varepsilon^2\mu_n$ and excitation amplitudes to $K_n = \varepsilon^2\hat{K}_n$ and $P_n = \varepsilon^3\hat{P}_n$. It should be noted that this scaling is consistent with the resonance notation [14]. After the scaling of coefficients, the system equation, with the small damping and small excitation amplitudes, assumes the following form:

$$\ddot{q}_n + 2\varepsilon^2\hat{\mu}_n \dot{q}_n + \omega_n^2 q_n + \alpha_n q_n^2 + \delta_n q_n^3 - \varepsilon^2\hat{K}_n q_n \cos\Omega t = \varepsilon^3\hat{P}_n \cos\Omega t \quad (30)$$

After introduction of the small parameter ε with which we scale space and time coordinates, the differential equation solution (30) is assumed as an expansion of functions with multiple variables:

$$q_n(t;\varepsilon) = \varepsilon q_{n,1}(T_0,T_1,T_2) + \varepsilon^2 q_{n,2}(T_0,T_1,T_2) + \varepsilon^3 q_{n,3}(T_0,T_1,T_2) \quad (31)$$

The parameter ε is additionally used to distinguish the motions occurring at the "fast" time scale $T_0 = t$, from the motions performed at "slower" time scales $T_1=\varepsilon t$, $T_2=\varepsilon^2 t$, etc. Changes at higher time scales are in fact small corrections of system response caused by non-linearity and damping, and by external and parametric excitations. It follows that the derivatives according to the independent variable t become partial derivatives of T_i variables:

$$\frac{\mathrm{d}}{\mathrm{d}t} = \frac{\mathrm{d}T_0}{\mathrm{d}t}\frac{\partial}{\partial T_0} + \frac{\mathrm{d}T_1}{\mathrm{d}t}\frac{\partial}{\partial T_1} + \ldots = D_0 + \varepsilon D_1 + \ldots$$

$$\frac{\mathrm{d}^2}{\mathrm{d}t^2} = D_0^2 + 2\varepsilon D_0 D_1 + \varepsilon^2\left(D_1^2 + 2D_0 D_2\right) + \ldots$$

The assumed solution (31) is inserted into the equation (30) and only the members of the order of ε^3 are retained. Then the expression members for the same powers of ε are equalised:

$$\varepsilon^1: \quad D_0^2 q_{n,1} + \omega_n^2 q_{n,1} = 0 \quad (32a)$$

$$\varepsilon^2: \quad D_0^2 q_{n,2} + \omega_n^2 q_{n,2} = -2D_0 D_1 q_{n,1} - \alpha_n q_{n,1}^2 \quad (32b)$$

$$\varepsilon^3: \quad D_0^2 q_{n,3} + \omega_n^2 q_{n,3} = \hat{P}_n \cos(\Omega T_0) + \hat{K}_n q_{n,1} \cos\Omega t - 2\hat{\mu}_n D_0 q_{n,1} - 2D_0 D_1 q_{n,2} - D_1^2 q_{n,1} - 2D_0 D_2 q_{n,1} - 2\alpha_n q_{n,1} q_{n,2} - \delta_n q_{n,1}^3 \quad (32c)$$

A general solution of the differential equation (32a) can be expressed in the following way:

$$q_{n,1} = A_n(T_1,T_2)e^{i\omega_n T_0} + \bar{A}_n(T_1,T_2)e^{-i\omega_n T_0} \quad (33)$$

where A is an unknown complex function while $\bar{A}$ is the conjugate function. Functions $A_n(T_1, T_2)$ and $\bar{A}_n(T_1,T_2)$ are determined from the condition that the solutions $q_{n,2}$ and $q_{n,3}$ must be periodic functions of the variable T_0. After insertion of the solution (33) into equation (32b) the following expression is obtained:

$$D_0^2 q_{n,2} + \omega_n^2 q_{n,2} = -2i\,\omega_n D_1 A_n e^{i\omega_n T_0} - \alpha_n A_n^2 e^{i2\omega_n T_0} - 2\alpha_n A_n \bar{A}_n + c.c. \quad (34)$$

where c.c. stands for complex conjugate pairs. Terms that contain the factor $e^{i\omega_n T_0}$ or $e^{-i\omega_n T_0}$ are called secular terms. Because of secular terms, the assumed solution (31) cannot be periodic and, after a certain period of time, the amplitude becomes infinite. Secular members must be eliminated to ensure compliance with the perturbation hierarchy, according to which the solution $q_{n,2}$ must be a small correction of the first solution. Thus the coefficients of secular terms in equation (34) must vanish:

$$-2i\,\omega_n D_1 A_n = 0$$

or:

$$D_1 A_n = 0 \quad (35)$$

Therefore, the function A_n does not depend on the variable T_1, i.e. $A_n = A_n(T_2)$. The same applies to its complex conjugate, $\bar{A}_n = \bar{A}_n(T_2)$. After elimination of secular terms, a particular solution for

the second order equation can be determined as follows:

$$q_{n,2} = \frac{\alpha_n}{3\omega_n^2} A_n^2 e^{i2\omega_n T_0} - \frac{2\alpha_n}{\omega_n^2} A_n \bar{A}_n + c.c. \tag{36}$$

As the system resonance depends on the vicinity of the system frequency ω_n and excitation frequency Ω, the parameter σ_n is introduced as it provide quantitative links between these values. The frequency nearness parameter σ_n is introduced so that secular terms can easier be recognised in the third order equation. The external or primary resonance occurs when the frequency of excitation is equal to one of the natural frequencies of the system, while the primary parametric resonance occurs when the excitation frequency is equal to twice the value of the natural frequency. Thus, depending on the frequency of excitation, two resonance cases are considered.

3.1.1. External resonance $\Omega \approx \omega_n$

At the third level of perturbation hierarchy, the changes along the time scale $T_2=\varepsilon^2 t$ are analysed and so, to ensure good consistency, the parameter σ_n, which defines the difference in excitation frequency and natural cable frequency, is scaled as follows:

$$\Omega = \omega_n + \varepsilon^2 \sigma_n \tag{37}$$

The expression (37) and solutions (33) and (36) are inserted in the third order equation (32c) and, together with the condition (35), we obtain:

$$\begin{aligned} &D_0^2 q_{n,3} + \omega_n^2 q_{n,3} = \frac{1}{2}\hat{P}_n e^{i\omega_n T_0 + i\sigma_n T_2} + \frac{1}{2}\hat{K}_n \bar{A}_n e^{i\sigma_n T_2} + \frac{1}{2}\hat{K}_n A_n e^{i2\omega_n T_0 + i\sigma_n T_2} \\ &-2i\hat{\mu}_n \omega_n A_n e^{i\omega_n T_0} - \frac{2\alpha_n^2 A_n^3}{3\omega_n^2} e^{i3\omega_n T_0} + \frac{10\alpha_n^2 A_n^2 \bar{A}_n}{3\omega_n^2} e^{i\omega_n T_0} \\ &-2i\omega_n D_2 A_n e^{i\omega_n T_0} - \delta_n A_n^3 e^{i3\omega_n T_0} - 3\delta_n A_n^2 \bar{A} e^{i\omega_n T_0} + c.c. \end{aligned} \tag{38}$$

The condition for regular and periodic solution is the elimination of secular terms from the right side of the equation (38):

$$\frac{1}{2}\hat{P}_n e^{i\sigma_n T_2} - 2i\hat{\mu}_n \omega_n A_n + \frac{10\alpha_n^2 A_n^2 \bar{A}_n}{3\omega_n^2} - 2i\omega_n D_2 A_n - 3\delta_n A_n^2 \bar{A}_n = 0 \tag{39}$$

Function A_n can be expressed in the polar form: $A_n = \frac{1}{2} a_n e^{i\beta_n}$, and $\bar{A}_n = \frac{1}{2} a_n e^{-i\beta_n}$, where a_n and β_n are real functions of the variable T_2. The real and imaginary parts of expression (39) are separated, and the label $\alpha_n^e = \delta_n - \frac{10}{9}\frac{\alpha_n^2}{\omega_n^2}$ is introduced. After solving the system of equations, modulation equations for the change in amplitude a_n and phase β_n are obtained:

$$\begin{aligned} a_n' &= -\hat{\mu}_n a_n + \frac{\hat{P}_n}{2\omega_n}\sin(\sigma_n T_2 - \beta_n) \\ \beta_n' &= -\frac{\hat{P}_n}{2\omega_n a_n}\cos(\sigma_n T_2 - \beta_n) + \frac{3}{8\omega_n}\alpha_n^e a_n^2 \end{aligned} \tag{40}$$

The equations (40) can be transformed into an autonomous system using the substitution $\beta_n = \sigma_n T_2 - \gamma_n$:

$$\begin{aligned} a_n' &= -\hat{\mu}_n a_n + \frac{\hat{P}_n}{2\omega_n}\sin\gamma_n \\ \gamma_n' &= \sigma_n + \frac{\hat{P}_n}{2\omega_n a_n}\cos\gamma_n - \frac{3}{8\omega_n}\alpha_n^e a_n^2 \end{aligned} \tag{41}$$

The equations (41) define the change of amplitude and phase of the nonlinear response for external resonance. The amplitude and phase value for steady motion are determined by inserting $a_n' = \gamma_n' = 0$ in expression (41):

$$\begin{aligned} 0 &= -\hat{\mu}_n a_n + \frac{\hat{P}_n}{2\omega_n}\sin\gamma_n \\ 0 &= \sigma_n + \frac{\hat{P}_n}{2\omega_n a_n}\cos\gamma_n - \frac{3}{8\omega_n}\alpha_n^e a_n^2 \end{aligned} \tag{42}$$

Once the phase γ_n is eliminated, the frequency-amplitude equation is defined as follows:

$$a_n^2\left[64\hat{\mu}_n^2\omega_n^2 + \left(8\sigma_n\omega_n - 3\alpha_n^e a_n^2\right)^2\right] = 16\hat{P}_n^2 \tag{43}$$

After expanding expression (43), we obtain:

$$9\alpha_n^{e\,2} a_n^6 - 48\alpha_n^e \sigma_n \omega_n a_n^4 + 64\omega_n^2\left(\hat{\mu}_n^2 + \sigma_n^2\right)a_n^2 - 16\hat{P}_n^2 = 0 \tag{44}$$

The number of real solutions to this bi-cubic equation depends on its discriminant values. If the system discriminant is negative, there is only one real solution for a_n^2 and, if it is positive, then there are three real solutions for a_n^2. The region of parameters for which multiple real solutions exist is the hysteric region of external resonances. Curves that separate these regions are determined by the vanishing discriminant, from which follows implicit equations:

$$\hat{P}_n^2 = \frac{64}{81}\left(\frac{\sigma_n\omega_n^3\left(9\hat{\mu}_n^2 + \sigma_n^2\right) \pm \omega_n^3\sqrt{\left(\sigma_n^2 - 3\mu_n^2\right)^3}}{\alpha_n^e}\right) \tag{45}$$

The point of intersection of the curves is determined by parameters values, as shown below:

$$\sigma_{kr} = \sqrt{3}\,\hat{\mu}_n \tag{46}$$

$$\hat{P}_{kr} = \pm\frac{16}{3}\sqrt{\frac{\hat{\mu}_n^3\omega_n^3}{\sqrt{3}\,\alpha_n^e}} \tag{47}$$

The character of equation (42) solutions can easily be examined using the local stability analysis, by specifying a small disturbance in the vicinity of a steady state, i.e. by setting small changes a_1 and γ_1 of the variables a_n and γ_n in the vicinity of a steady state (a_0, γ_0):

$$\begin{aligned} a_n &= a_0 + a_1 \\ \gamma_n &= \gamma_0 + \gamma_1 \end{aligned} \tag{48}$$

After substitution in the modulation equations (41), and by retaining only linear terms, we have:

$$a_1' = -\hat{\mu}_n a_1 + \left(\frac{\hat{P}_n}{2\omega_n}\cos\gamma_0\right)\gamma_1,$$
$$\gamma_1' = -\left(\frac{3}{4\omega_n}\alpha_n^e a_0 + \frac{\hat{P}_n}{2\omega_n a_0^2}\cos\gamma_0\right)a_1 - \left(\frac{\hat{P}_n}{2\omega_n a_0}\sin\gamma_0\right)\gamma_1 \quad (49)$$

The stability of motion depends on eigenvalues of the coefficient matrix on the right side of expression (49). Hence, the motion is unstable for:

$$\mu_n^2 + \left(\sigma_n - \frac{3}{8\omega_n}\alpha_n^e a_0^2\right)\left(\sigma_n - \frac{9}{8\omega_n}\alpha_n^e a_0^2\right) < 0, \quad (50)$$

while otherwise it is considered stable. The final solution for the steady state function and second approximation is:

$$q(t) = \varepsilon a_n \cos(\Omega t - \gamma_n) + \varepsilon^2 a_n^2 \frac{\alpha_n}{6\omega_n^2}\left(\cos(2\Omega t - 2\gamma_n) - 3\right) + O(\varepsilon^3) \quad (51)$$

This solution depends on the powers of coefficients $(\varepsilon a_n)^i$, and if the amplitude is small, one can set $\varepsilon = 1$ and consider a_n as the perturbation parameter [15]. It should be noted that scaled coefficients do not change in this case.

3.1.2. Parametric resonance $\Omega \approx 2\omega_n$

The primary parametric resonance in the system occurs when the excitation frequency is close to the double value of the natural system frequency ω_n, and so the following relation is introduced:

$$\Omega = 2\omega_n + \varepsilon^2\sigma_n \quad (52)$$

The expression (52), and solutions (33) and (36), are included in the third order equation (32c) and, together with the condition (35), we obtain:

$$\begin{aligned} &D_0^2 q_{n,3} + \omega_n^2 q_{n,3} = \frac{1}{2}\hat{P}_n e^{i2\omega_n T_0 + i\sigma_n T_2} + \frac{1}{2}\hat{K}_n \bar{A}_n e^{i\omega_n T_0 + i\sigma_n T_2} + \frac{1}{2}K_n A_n e^{i3\omega_n T_0 + i\sigma_n T_2} \\ &-2i\hat{\mu}_n\omega_n A_n e^{i\omega_n T_0} - \frac{2\alpha_n^2 A_n^3}{3\omega_n^2}e^{i3\omega_n T_0} + \frac{10\alpha_n^2 A_n^2 \bar{A}_n}{3\omega_n^2}e^{i\omega_n T_0} \\ &-2i\omega_n D_2 A_n e^{i\omega_n T_0} - \delta_n A_n^3 e^{i3\omega_n T_0} - 3\delta_n A_n^2 \bar{A} e^{i\omega_n T_0} + c.c. \end{aligned} \quad (53)$$

In order to obtain a regular periodic solution, the coefficients that generate secular terms must be eliminated:

$$\frac{1}{2}\hat{K}_n e^{i\sigma_n T_2} - 2i\hat{\mu}_n\omega_n A_n + \frac{10\alpha_n^2 A_n^2 \bar{A}_n}{3\omega_n^2} - 2i\omega_n D_2 A_n - 3\delta_n A_n^2 \bar{A}_n = 0 \quad (54)$$

By expressing functions A_n and $\bar{A}_n$ in polar form, modulation equations for the amplitude a_n and the phase β_n of parametric oscillations, are determined by:

$$a_n' = -\hat{\mu}_n a_n + \frac{\hat{K}_n a_n}{4\omega_n}\sin(\sigma_n T_2 - 2\beta_n)$$
$$\beta_n' = -\frac{\hat{K}_n}{4\omega_n}\cos(\sigma_n T_2 - 2\beta_n) + \frac{3}{8\omega_n}\alpha_n^e a_n^2 \quad (55)$$

By transforming equations in an autonomous system with the substitution $2\beta_n = \sigma_n T_2 - \gamma_n$ we obtain:

$$a_n' = -\hat{\mu}_n a_n + \frac{\hat{K}_n a_n}{4\omega_n}\sin\gamma_n$$
$$\gamma_n' = \sigma_n + \frac{\hat{K}_n}{2\omega_n}\cos\gamma_n - \frac{3}{4\omega_n}\alpha_n^e a_n^2 \quad (56)$$

The system equilibrium for $a_n' = \gamma_n' = 0$, is defined with equations:

$$0 = -\hat{\mu}_n a_n + \frac{\hat{K}_n a_n}{4\omega_n}\sin\gamma_n$$
$$0 = \sigma_n + \frac{\hat{K}_n}{2\omega_n}\cos\gamma_n - \frac{3}{4\omega_n}\alpha_n^e a_n^2 \quad (57)$$

Hence, the explicit expression for the amplitude of parametric oscillations is:

$$a_n^2 = \frac{4\sigma_n\omega_n}{3\alpha_n^e} \pm \frac{2}{3\alpha_n^e}\left(\hat{K}_n^2 - 16\hat{\mu}_n^2\omega_n^2\right)^{1/2} \quad (58)$$

The expression (58) yields the necessary condition for the size of the parametric excitation amplitude:

$$\hat{K}_n \geq 4\hat{\mu}_n\omega_n \quad (59)$$

The region of parametric resonance can be determined from the condition $a_n^2 > 0$ as follows:

$$\sigma_n > \pm\frac{1}{2\omega_n}\left(\hat{K}_n^2 - 16\hat{\mu}_n^2\omega_n^2\right)^{1/2} \quad (60)$$

To analyse the stability of solutions (57), small perturbations (a_1, γ_1) are set in the vicinity of the equilibrium point (a_0, γ_0). After insertion in modulation equations (56), and after retaining only linear terms for variables a_1 and γ_1, we obtain:

$$a_1' = \left(\frac{K_n a_0}{4\omega_n}\cos\gamma_0\right)\gamma_1$$
$$\gamma_1' = -\left(\frac{3\alpha_n^e}{2\omega_n}a_0\right)a_1 - 2\mu_n\gamma_1 \quad (61)$$

Motion is unstable for:

$$\sigma_n - \frac{3\alpha_n^e}{4\omega_n}a_n^2 > 0 \quad (62)$$

The final solution of function for the steady state of parametric oscillations in the second approximation is:

$$q = \varepsilon a_n \cos\left(\frac{1}{2}(\Omega t - \gamma_n)\right) + \varepsilon^2 a_n^2 \frac{\alpha_n}{6\omega_n^2}\left(\cos(\Omega t - \gamma_n) - 3\right) + O(\varepsilon^3) \quad (63)$$

4. Numerical model

In the numerical model, spatial derivatives are approximated with central differences. The cable is spatially discretized with *N-1* segments Δx in length, where *N* is the number of discrete nodes. Central differences of *w* in the spatial derivatives are:

$$\frac{\partial w}{\partial x} \approx \frac{W_{i+1} - W_{i-1}}{2\Delta x} = W_{D1,i}$$
$$\frac{\partial^2 w}{\partial x^2} \approx \frac{W_{i+1} - 2W_i + W_{i-1}}{\Delta x^2} = W_{D2,i} \quad (64)$$

where index *i* refers to the spatial node (*i=1,2,3,...M*) while indices *D1* and *D2* are the first and second approximations of spatial derivatives of *w* for the node *i*. The Simpson's rule is applied for the approximation of integral in equation (21):

$$S=\int_0^1\left(z'w'+\tfrac{1}{2}w'^2\right)\mathrm{d}x\approx\frac{\Delta x}{3}\left(s_1+4\sum_{i=1}^{\frac{N-1}{2}}s_{2i}+2\sum_{i=1}^{\frac{N-1}{2}-1}s_{2i+1}+s_N\right) \quad (65)$$

where:

$$s_i=4\nu\left(1-2(i-1)\Delta x\right)W_{D1,i}+\frac{1}{2}W_{D1,i}^2 \quad (66)$$

After the finite difference discretization, the equation system is expressed as:

$$W_{D2,i}+\eta\left(W_{D2,i}-8\nu\right)\left(S-\Delta_u\cos\left(\Omega j\Delta t\right)\right)=\ddot{W}_i+2\mu\dot{W}_i \quad (67)$$

The time integration of equations is conducted using the iterative Predictor-Corrector algorithm for the time step of $\Delta t=0{,}002$ [16]. The cable model is discretized with *N=53* nodes, which are successively numbered, and so the first node corresponding to the moving support is *i=1*, while it is *i=53* for the fixed support. The transverse displacement of support *A* is given by the function $W_1=\Delta_p\cos(\Omega j\Delta t)$, where *j* represents the time integration step.

5. Examples

Dimensionless parameters η and ν are selected to fit cable parameters of cable stayed bridges. The static deformation of a typical stay cable ranges from 0,2 to 0,4 %, while the sag to span ratio varies from 0,01 to 0,5 % [17]. These are highly pretensioned cables, and so the parabolic approximation that was used to derive analytic expressions can be applied in this case as well. The parameter chosen for cable stretching is $\eta = 400$, and the value of $\nu = 0.002$ is adopted for the sag-to-span ratio. Therefore, the Irvine parameter is $\lambda^2 = 0.1024$. The relative modal damping of $\xi = 0.5$ % is used for all oscillation modes. Only the lower order oscillations will be analysed, i.e. the external resonance of the first and second modes, and the parametric resonance of the first mode, for the case when there is no interaction between the modes.

5.1. External resonance

The first symmetric mode $\phi_1(x)$ is initially used for system reduction. In this case, both support displacements cause external excitation since the coefficients h_1 and p_1 are different from zero. Figure 4 shows external resonance regions for different longitudinal and transverse support displacement relations (Δ_p and Δ_u). Different resonance regions that are characteristic for a nonlinear system are marked in the left-side figure. For the values $\sigma_1 > \sigma_{kr}$, the system's response depends on the excitation parameters only, i.e. the higher the frequency and amplitude of the excitation, the larger the response amplitude. There are three resonance regions for $\sigma_1 > \sigma_{kr}$, and the expression (45) defines boundary curves of the hysteresis region. In the region of low-amplitude resonance, the linear system provides a good approximation of the oscillation amplitude [11]. Above the hysteresis region, there is a region of high response amplitudes. If parameters correspond to the hysteresis region, the system can have either high or low response amplitudes. The final solution will depend on initial conditions, i.e. on the response history.

Figures 5, 6, and 7 display steady state amplitude curves as a function of the excitation frequency/amplitude. Asymptotic solutions obtained by MMS are checked by direct numerical integration (NI) of equation (28) using the *Wolfram Mathematica* software. After achieving the steady state response, the amplitude of oscillation is determined, and the excitation frequency/amplitude is changed. The label × marks the frequency/amplitude change from lower toward the higher values, and the label + designates the change from higher to lower values. For the model that is formulated with finite differences (FD), once the steady state response is achieved, the maximum displacement of the node in mid-span (node 27) is taken to be the amplitude caused by external resonance. Empty circles represent FD results for homogeneous initial conditions

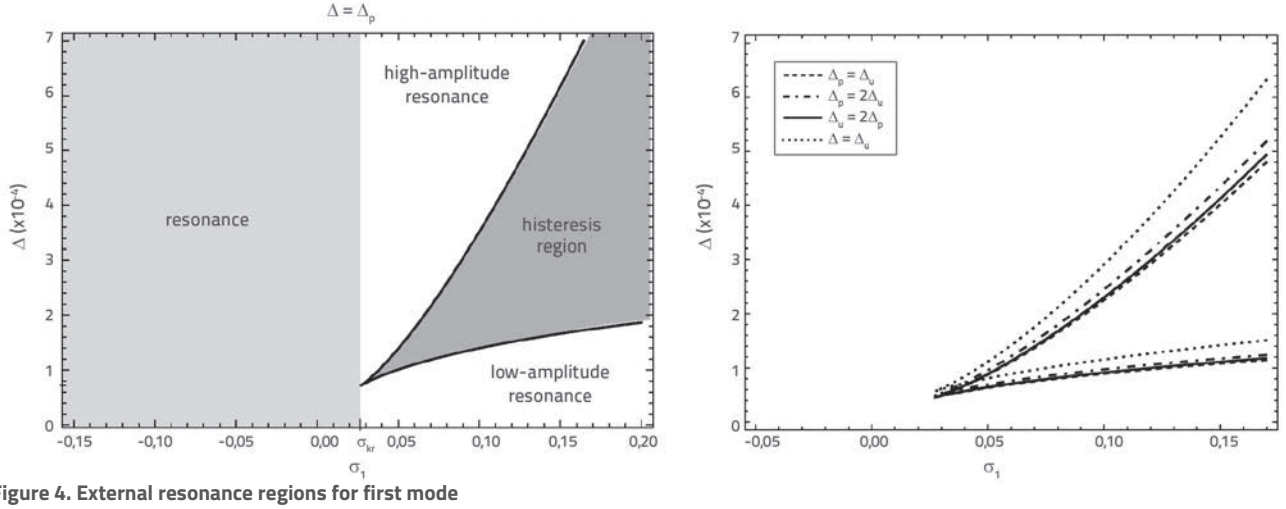

Figure 4. External resonance regions for first mode

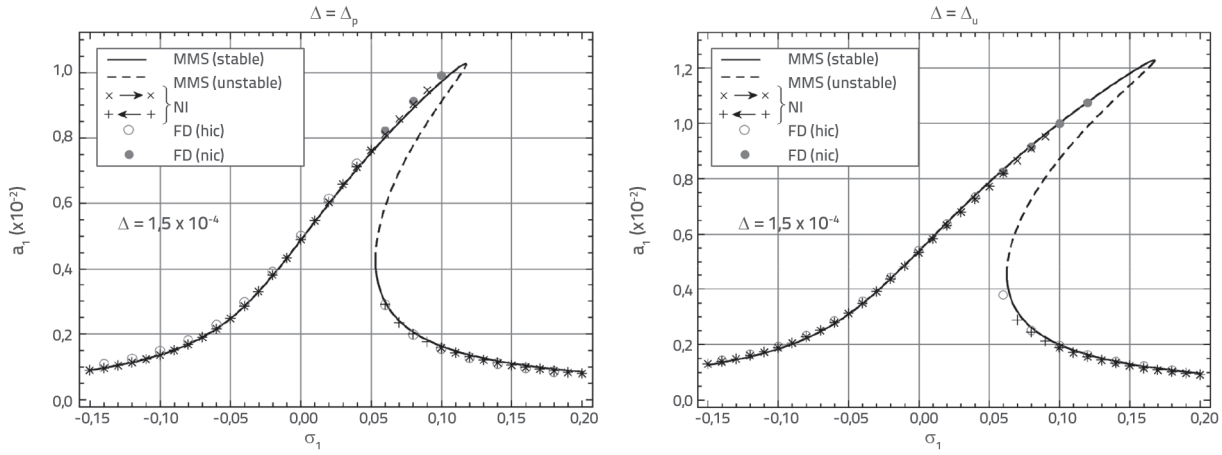

Figure 5. Frequency-amplitude curves for constant excitation amplitude

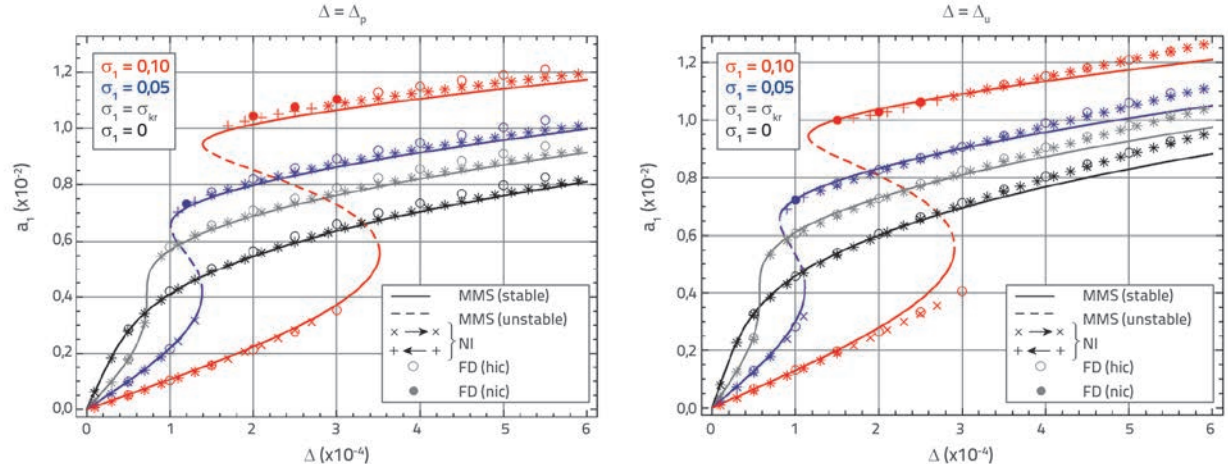

Figure 6. Amplitude curves for constant excitation frequency

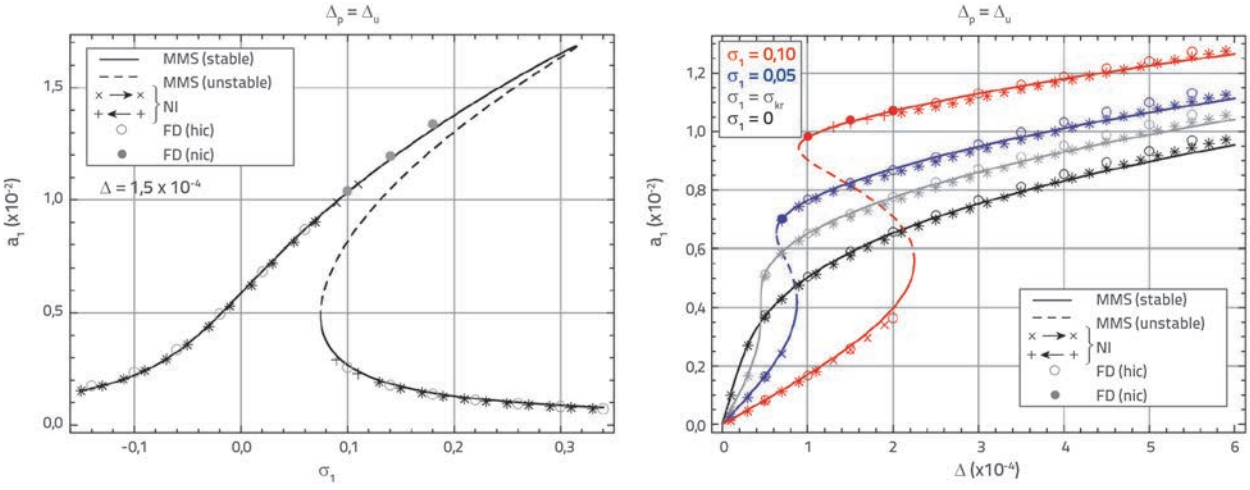

Figure 7. Amplitude curves for simultaneous longitudinal and transverse support displacement

(hic), while full circles stand for inhomogeneous initial conditions (nic). Initial conditions are set in the vicinity of the equilibrium state.

For small values of support motion, the numerical analysis results agree very well with the results obtained by MMS. Figure 6 shows that a minor deviation can only be noted for larger response/excitation values. The advantage of the proposed analytic model lies in the fact that it does not neglect the curved static profile of the cable. This example shows that the longitudinal component of support motion also causes external resonance of the first

mode. It can also be noted that, for given cable parameters, its amplitude is of same order of magnitude as the response amplitude caused by transverse component of support motion.
Figure 7 displays amplitude curves for the simultaneous longitudinal and transverse support motion. The total amplitude defined by expression (29) is greater than in the previous two cases, and hysteresis region shifts toward low values of support displacement Δ. Equation (29) also shows that the change of sign in one support component causes the change of the system resonance region.

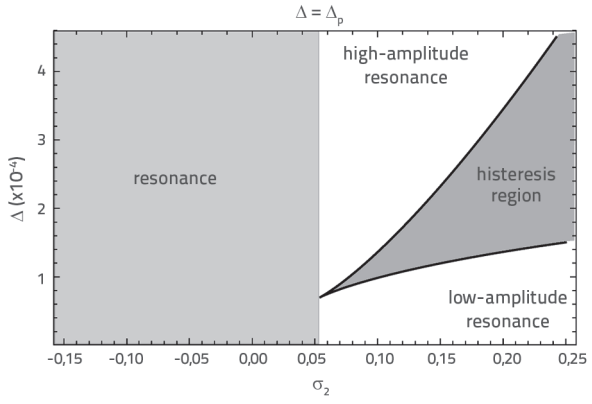

Figure 8. External resonance regions for second mode

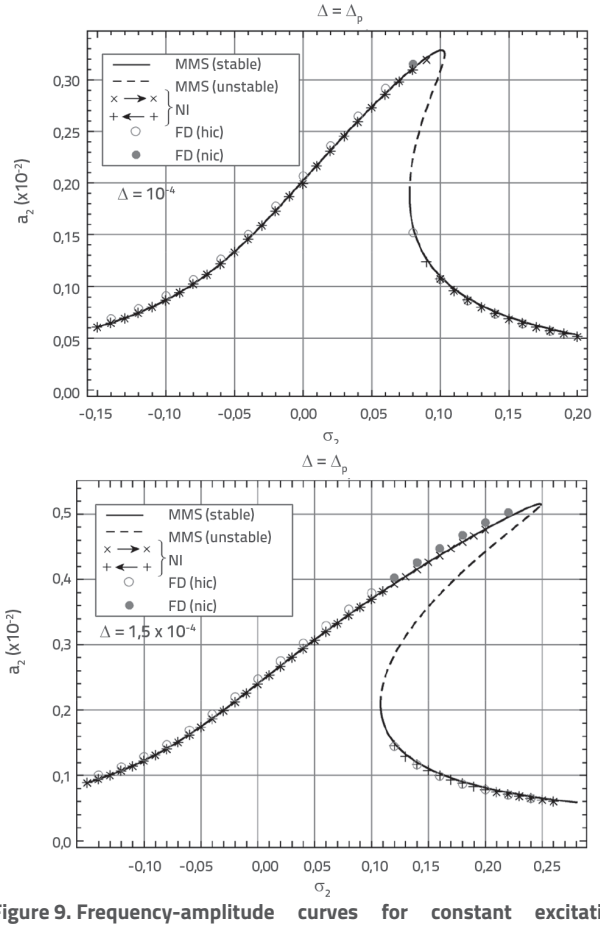

Figure 9. Frequency-amplitude curves for constant excitation amplitude

For system reduction by the second mode of oscillation, the excitation coefficient h_2 vanishes because the function $\phi_2(x)$ is asymmetric. Accordingly, the second mode oscillation is caused by the transverse support motion component only. The second mode resonance regions are presented in Figure 8. In FD model, the amplitude is represented by maximum displacement of the node in one quarter of the span (node 14). The second mode resonance has smaller amplitudes compared to response amplitudes in the case of the first mode resonance, because the second mode deformation requires higher energy consumption (Figures 9 and 10). Here also a good agreement is achieved between numerical and analytic results, especially for low excitation/response values.

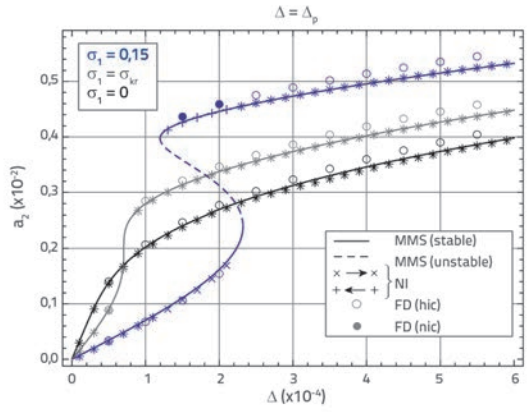

Figure 10. Amplitude curves for constant excitation frequency

5.2. Parametric resonance

The parametric excitation is caused by the longitudinal support displacement only. The region of parameters for which parametric oscillations are possible is defined by expressions (59) and (60). Boundary curves do not depend on the nonlinear coefficient and are analogous to the parametric resonance region expressions defined for the linear system derived from the Mathieu's equation. However, the nonlinear system response in resonance regions is quite different compared to the linear system response.
Three parametric resonance regions displayed in figure 11 are defined by expressions (59) and (60). No parametric oscillations can occur in the unshaded region, regardless of initial conditions. If parameters correspond to the primary region of parametric resonance in which response amplitude of the linear system is infinite, the nonlinear system amplitudes have a final value and, consequently, the limit cycle is reached. After the right boundary, there is a hysteresis region of parametric oscillation where the system response can be trivial, or it is periodic with a high oscillation amplitude. Initial conditions or response history determine whether parametric oscillations will in fact occur. In the linear system, parametric oscillations are not possible for parameter values corresponding to the hysteresis region. This is a rare case of nontrivial solution of

nonlinear system in the region in which the response of linear system is trivial [14].

Parametric oscillation amplitudes for cables are shown in Figures 12 and 13. These figures also show matching results of analytic and numerical models.

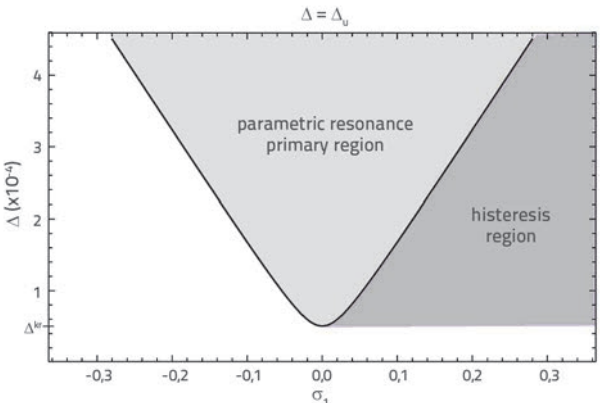

Figure 11. Parametric resonance regions for first mode

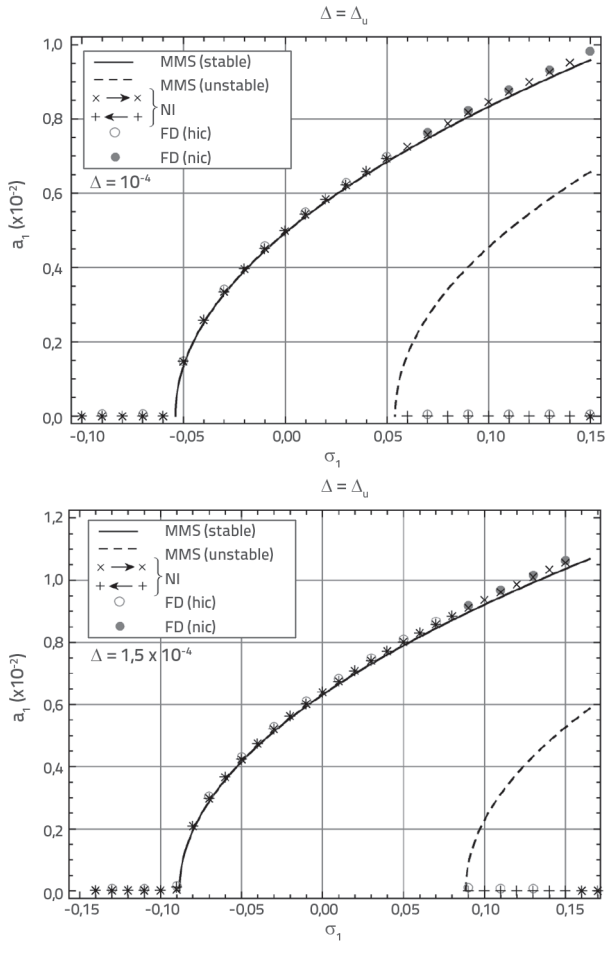

Figure 12. Frequency-amplitude curves for constant excitation amplitude

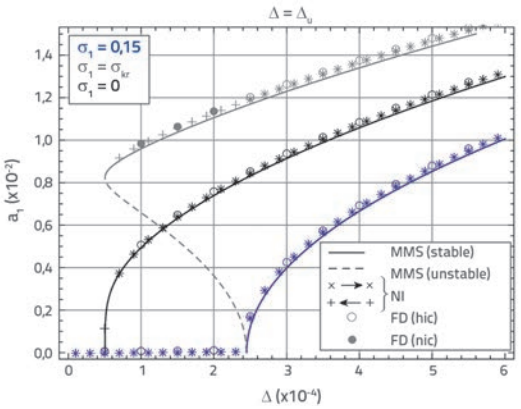

Figure 13. Amplitude curves for constant excitation frequency

6. Conclusion

An analytic procedure for modelling cable oscillations due to support motion is presented in this paper. The procedure is based on the assumption of quasi-static cable stretching, and on the concept of composed motion. Besides the cubic nonlinearity caused by cable stretching, quadratic nonlinearities are also included in the formulation by taking into account the function of curved static profile, which is neglected in reference papers, and is due to the influence of geometry in the equilibrium position. This influence has included in the analytic model the occurrence of external transverse oscillations due to longitudinal support displacement. Systems that ignore the influence of curved geometry include only cubic nonlinearities (taut wire), and so longitudinal support displacements cause parametric oscillations only. The analysis of the reduced system equation shows that the coefficient of external excitation due to longitudinal component of support motion vanishes for asymmetric trial functions and so, in this case, oscillations occur only due to the transverse component of support motion.

In the selected example, the ratio of system frequencies amounts to $2\bar{\omega}_1 / \bar{\omega}_2 = 1{,}004$. Thus, for the excitation frequency of $\Omega \approx 2\omega_1 \approx \omega_2$ results are shown only when one of the support displacement component acts. This allowed us to separately study external resonance of the second mode and parametric resonance of the first mode. In the case when both components are present, simultaneous external and parametric resonance conditions are met, and so the nonlinear model, which is defined by equation (26), needs to include all excited modes.

The comparison of analytic and numerical results shows a very good correspondence of results and a high accuracy of asymptotic solutions. The advantage of using the MMS procedure is quite obvious, as analytic solutions allow simple determination of the response amplitude, and a more transparent qualitative analysis of results.

The study shows that even a very small support motion can cause large response amplitudes for a particular region of excitation and system parameters.

REFERENCES

[1] SETRA: Cable Stays; Recommendation of French Interministerial Commision on Prestressing, Center des Techniques des Ouvraes d"Art, Bagneux Cedex, France, 2002.

[2] Rega, G.: Nonlinear vibrations of suspended cables – part I: Modeling and analysis, *Applied Mechanics Review* 57 (2004) 6, pp. 443-478.

[3] Irvine, H.M., Caughey, T.K.: The Linear Theory of Free Vibrations of a Suspended Cable, *Proceedings of the Royal Society Series A 341*, pp. 299-315, 1974., http://dx.doi.org/10.1098/rspa.1974.0189

[4] Irvine, H.M.: *Cable Structures*, The MIT Press, Cambridge, Mass., 1981.

[5] Triantafyllou, M.S.: The dynamic of taut inclined cables, *Quarterly Journal of Mechanics and Applied Mathematics* 37 (1984) 3, pp. 421-440.

[6] Wu, Q., Takahashi, K., Nakamura, S.: Formulae for frequencies and modes of in-plane vibrations of small-sag inclined cables, *Journal of Sound and Vibrations* 279 (2005), pp. 1155-1169, http://dx.doi.org/10.1016/j.jsv.2004.01.004

[7] Rega, G., Srinil, N., Alaggio, R.: Experimental and numerical studies of inclined cables: free and parametrically-forced vibrations, *Journal of Theoretical and Applied Mechanics* 46 (2008.) 3, pp. 621-640.

[8] Caetano, E.: Indirect excitation of stays on cable-stayed bridges, *Fourth International Symposium on Cable Dynamics*, Montreal, Canada, pp. 129-136, 2001.

[9] Lilien, J.L., Pinto da Costa, A.: Vibration amplitudes caused by parametric excitation of cable stayed structures, *Journal of Sound and Vibration* 174 (1994) 1, pp. 69-90.

[10] Pinto da Costa, A., Martins, J.A.C., Branco, F., Lilien, J.L.: Oscillations of Bridge Stay Cables Induced by Periondic Motions of Deck and/or Towers, *Journal of Engineering Mechanics* 122 (1996) 7, pp. 613-622.

[11] Douthe, C.E., Gantes, C.J.: Investigation of coupling between external and parametric resonances in small sagged inclined cables, *III ECCOMAS Thematic Conference on Computational Methods in Structural Dynamics and Earthquake Engineering*, Corfu, 2011.

[12] Jakobsen, P.: Introduction to the method of multiple scales, Cornell University Library, 2014, URL:http://arxiv.org/abs/1312.3651v2

[13] Marinca, V., Nicolae, H.: *Nonlinear Dynamical Systems in Engineering*, Springer, 2011., http://dx.doi.org/10.1007/978-3-642-22735-6

[14] Nayfeh, A.H., Mook, D.T.: *Nonlinear Oscillations*, John Wiley & Sons Inc., 1995., http://dx.doi.org/10.1002/9783527617586

[15] Nayfeh, A.H.: *Introduction to Perturbation Techniques*, John Wiley & Sons Inc., 1993.

[16] Nikolić, M., Raduka, V.: Numerical investigation of cable parametric vibration, *11th International Conference on Vibration Problems*, Lisbon, Paper No. 158, 2013.

[17] Achkire, Y.: Active Tendon Control of Cable-Stayed Bridges, Universite Libre de Bruxelles, Active Structures Laboratory, Dissertation, Belgium, 1997.